Research on pH-responsive Antibacterial Materials Using Citral-modified Zinc Oxide Nanoparticles

Yanan Fan[a1],Qixiang Xu[a1], Keyu Ren[a], Mengge Zhai[a], Guozheng Xing[a], Yishan Song[a, b,c,]* Yongheng Zhu[a,b,c,]*

[a] *College of Food Science and Technology, Shanghai Ocean University, Shanghai 201306, P.R. China*

[b] *Shanghai Engineering Research Center of Aquatic-Product Processing & Preservation, Shanghai 201306, P.R. China*

[c] *Laboratory of Quality and Safety Risk Assessment for Aquatic Products on Storage and Preservation (Shanghai), Ministry of Agriculture and Rural Affairs, Shanghai 201306, China*

Yanan Fan and Qixiang Xu are the co-first authors of the paper.

* Corresponding authors:

Yishan Song, Yonghong Zhu, No.999, Huchenghuan Rd, Nanhui New City, Shanghai, P.R. China: 201306, fax: +86-21-61900365, *e-mail* yssong@shou.edu.cn (Ys. Song) ; yhzhu@shou.edu.cn (Yh. Zhu)

E-mail addresses: fynwsq@163.com (Yn. Fan), qxxu@shou.edu.cn (Qx. Xu), lu18337007211@163.com(Ky. Ren), mengge0309@163.com (Mg. Zhai), 995276929@qq.com (Gz. Xing)

Abstract:

With the deepening of the harm of foodborne pathogens to human health and the increasing attention of people to healthy diet, novel food antimicrobial agents have been widely studied by researchers as hotspots. In this study, three different morphologies of citral-modified ZnO nanopaticles antimicrobial materials were prepared, and the citral-modified porous ZnO nanorods antimicrobial materials with the highest loading (60.35%) and the strongest inhibitory effect (MIC = 0.2 mg/mL ~ 0.1 mg/mL) were screened out through a series of characterization and bacterial inhibition experiments. This novel antimicrobial material has excellent and long-lasting antimicrobial properties. It inhibits *Escherichia coli* by 100% when stowed at 25°C and protected from light for 10 days, and inhibits the growth of *E. coli* by 58.17% after being stowed under the same conditions for 60 days. Furthermore, we tested the pH change during 24 hours of *E. coli* growth and pH responsiveness of the materials. The results demonstrated that under the acid-producing condition of *E. coli* growth, the pH-sensitive imine bond (-CH=N-) formed by the condensation of amino of functionalized ZnO nanoparticles and citral was hydrolyzed to release the citral, thus indicating that the release mechanism of citral in the antibacterial material was pH-sensitive acid release in the process. The antibacterial materials in this study have broad application prospects in the field of food production and packaging in the future. Meanwhile, this study provides a theoretical basis for guaranteeing food quality and safety.

Keywords: Foodborne pathogen; Sterilization; PH-sensitive; Imine bond; Food safety.

1. Introduction

The quality and safety of food are closely related to people's lives. Microbiological, chemical, climatic, and water activities can affect the safety of food, and the foodborne pathogens among them are particularly damageful, as they not only lead to reduced food quality but also cause foodborne diseases(Aladhadh 2023). Nowadays, not only developing countries, but also developed countries are experiencing serious incidents of food-based pathogenic bacteria pollution(Mengistu and Tolera 2020, Hailu, Helmy et al. 2021). Food-borne microorganisms can cause bacterial infections and food poisoning, threatening human health and hindering economic prosperity. Therefore, the development of a fast and effective sterilization method for pathogenic bacteria in food is essential. Traditional sterilization techniques may have adverse effects on the texture and flavor of food products，but newer sterilization techniques like plasma sterilization and pulsed electric field sterilization are challenging to implement on a large scale in industrial production due to their high economic costs and energy consumption(Guo, Azam et al. 2022, Soni and Brightwell 2022, WANG Xiaodong 2022). The most common method of inhibiting the growth of microorganisms in food is to use bacteriostatic agents(ZHAO Dongxue 2021). However, when synthetic bacteriostats are used for a long time, microorganisms may develop resistance to them, which limits the large-scale application of synthetic bacteriostats in industry, and also promotes the research of natural antimicrobial materials as bacteriostats.

Essential oils are secondary metabolites of plants and they can be obtained by fermentation or extraction, and the method of steam distillation is the most common method of commercial production of essential oils(Ghasemy-piranloo, Kavousi et al. 2020). Essential oils are known for their antibacterial, antioxidant, and anticancer activities and have been rated globally as safe, non-toxic, and effective natural antibacterial substances(Tajkarimi, Ibrahim et al. 2010, Chen, Shang et al. 2023, Meenu, Padhan et al. 2023, Mohamed Abdoul-Latif, Ainane et al. 2023). The antimicrobial mechanism of essential oils has been shown to involve the disruption of bacterial cell membranes and the reduction of cell permeability(Kachur and Suntres 2020). It has also indicated in previous studies to be by affecting intracellular ion transport and the interaction between membrane proteins and compounds(Yin, Liang et al. 2022). Alternatively, the mechanism affects the active sites of enzymatic reactions in the bacterial cell to produce an antibacterial effect(Kuttithodi, Narayanankutty et al. 2023). All of these effects disrupt the normal growth process of the bacterial cell, ultimately leading to cell death. Essential oils have been recognized as excellent antibacterial ingredients due to their various advantages, but their volatility, photosensitivity, and water resistance limit their use in terms of antibacterial (Al-Maqtari, Rehman et al. 2021). Therefore, some researchers are dedicated to developing more scientific and reasonable methods, such as preparing relatively stable active coatings containing essential oils, emulsifying essential oils into emulsions, and encapsulating essential oils in carriers for controlled release, in order to reduce the volatility of essential oils and enhance their active utilization(Peighambardoust, Yaghoubi et al. 2022, Ren, Lim et al. 2022). Wanting et al. prepared nanoparticles using the counter-solvent method with cysteine-chitosan and zein as wall materials and capsaicin as the core material. The synthesized nanomaterials was spherical in shape with a uniform size distribution, and the release rate of capsaicin was only (40.08±4.28)% after 4 hours of simulated digestion in vitro, which showed excellent pH stability and ionic strength stability(YIN Wanting 2023). In this study, the essential oils were loaded by controllable chemical bond bonding to the nanocarriers rather than encapsulation , which would significantly decrease the impact of environment on the active substances in free form and minimize the negative impact of essential oils on food organoleptics when applied to food packaging.

Nanoparticles (NPs) are a branch of nanotechnology that studies small particle materials ranging in size from 1 nm to 100 nm(Khan, Sadia et al. 2022). Due to their small size, NPs have the larger specific surface area and exhibit unique characteristics(Kavitha, Doss et al. 2023). Some nano-materials, such as nano-liposomes(Siyadatpanah, Norouzi et al. 2023), nano-emulsion(Nie, Pan et al. 2023), biopolymeric nanoparticles(Vodyashkin, Kezimana et al. 2022), could be used as antibacterial carriers to encapsulate essential oil molecules, thereby enhancing the durability of their antibacterial ability. ZnO nanoparticles (ZnO-NPs) have the characteristic of small particle size, large specific surface area, and diverse micromorphological structures, as well as having unique properties such as pyroelectricity, semiconductivity, and high scope for modification development (Wang Xuewen, Xu Zhengyan et al. 2022). In addition, ZnO-NPs have been recognized as Generally Recognized As Safe (GRAS) by the US Food and Drug Administration (FDA) due to their safe and non-toxic properties(Mishra, Mishra et al. 2017). ZnO-NPs possess certain antimicrobial activity by themselves, and their physicochemical properties

can predict their antimicrobial and toxicological effects(Czyzowska and Barbasz 2022). The properties of ZnO-NPs, including morphology, particle size or particle size distribution, porosity, and specific surface area, affect the antimicrobial activity(Yu, Li et al. 2020). The particle size and particle size distribution level of ZnO- NPs are the key parameters to determine the antimicrobial activity against pathogenic microorganisms(Sharma, Kumar et al. 2019). In recent years, ZnO-NPs have been widely utilized in various fields such as optical, medical, agricultural, and horticultural industries(Du, Zhang et al. 2019, Samart and Chutipaijit 2019, Yoon and Oh 2021, Costa, Abucafy et al. 2023).

The imine bond in chemical reaction is a pH-responsive covalent bond that is stable at neutral pH (~7.4) and easily hydrolyzed in acidic environments(Zhou, Zhai et al. 2023), and the rate of hydrolysis is positively correlated with environment acidity, which has been extensively practised in biomedical hydrogels and polymeric micelles(Zhang, He et al. 2018, Zhang, Niu et al. 2023). Jiawei et al. prepared aldehyde-chitosan Schiff base compounds using chitosan and five natural aldehydes, which had better antimicrobial activity at pH 5 compared to pH 7. This was attributed to the hydrolysis and breaking of the imine bond to release more aldehydes at pH 5. In addition, the aldehyde-chitosan Schiff base compounds were able to extend the shelf life of broccoli (from 4 to 5-7 days) and reduce the loss of water from the broccoli, which resulted in freshness preservation of the broccoli(Lin, Meng et al. 2023). The other study fabricated smart antifungal films by grafting aldehydes (cinnamaldehyde, citral, hydrogenated cinnamaldehyde, and citronellal) onto the surface of chitosan films by enabling the acid-catalyzed condensation of the carbonyl group with the amino group to form an imine bond. The results of antifungal activity testing in vitro of this dynamic film against two fungi, *Pseudomonas expansa* and *Staphylococcus griseus*, showed that all the films exhibited antifungal activity, and their antifungal activity was attributed to the aldehydes released after the imine bond was broken in an acidic environment(Heras-Mozos, Hernández et al. 2022).

Based on the current research status, we designed a pH-responsive intelligent release strategy for zinc oxide nanomaterials modified with essential oil. Since essential oil molecules in encapsulated form will be sensitive to the environment during storage, we introduced amino groups onto the surface of ZnO-NPs to condense with aldehyde groups to form imine bonds, which controlling the release of essential oil molecules and achieving the desired antibacterial effect. In this antibacterial material, antimicrobial carriers were zinc oxide nanoparticles, imine bonds were employed as 'control key' of the release process, and citral was utilized as an effective component to exert antibacterial activity. When there is a small amount of *E. coli* in the system, only a limited quantity of acid metabolites is produced. This leads to a slight decrease in the system's pH and opening of a tiny amount of imine bonds, resulting in the release of a small number of essential oil molecules to inhibit the bacteria. Conversely, when there is a high concentration of *E. coli*, a larger quantity of acid metabolites is produced, causing a significant decrease in the system's pH. This condition is sufficient for the imine bond to break completely and release large amounts of essential oil. The experimental data on antimicrobial activity indicated that the synthesized materials' adaptive pH-responsive antimicrobial system can be utilized to inhibit *E. coli.*

2. Materials and Methods

2.1 Reagents and culture medium

Zinc nitrate hexahydrate ($Zn(NO_3)_2 \cdot 6H_2O$, 99%), zinc acetate dihydrate ($(C_4H_6O_4)_2 \cdot Zn \cdot 2H_2O$, 99%), hexadecyl trimethyl ammonium bromide (CTAB, 99%), β-Cyclodextrin (β-CD), diethylene glycol (DEG, 98.9%), ammonium hydroxide（$NH_3 \cdot H_2O$, 99.99%）, (3-Aminopropyl) triethoxysilane (3-APTES, 99%), ethanol absolute (99.8%), Dimethyl sulfoxide (DMSO, 99%), glutaraldehyde 25% water solution (25%), sodium chloride (NaCl, 99％), Tryptose Soya Agar (TSA), Trypticase Soy Broth (TSB), commercialization none Fixed nano - zinc oxide were purchased from Aladdin Biochemical Technology Co., Ltd. (Shanghai, China)

E. coli strains were obtained from Shanghai Ocean University. After the initial activation, the *E. coli* strains were stored in a broth containing 25% glycerol and soybean trypsin at a temperature of -80°C. The strains were inoculated into a liquid medium and incubated in a constant temperature

incubator at 37°C for 24 hours. The concentration of the bacterial solution was adjusted to approximately 10^6 CFU/mL through gradient dilution before each antibacterial experiment.

2.2 Preparation and modification of ZnO-NPs

Preparation of ZnO nanorods (ZNR). ZNR were prepared with reference to the modified literature method(Ouyang, Ren et al. 2021). 2.3 g of CTAB, 8.0 g of β-CD, and 2.0 g of $NH_3 \cdot H_2O$ were mixed and dissolved in 100 mL of deionized water. The mixture was then ultrasonically dispersed for 30 minutes until it was completely dissolved. Then, 8.0 g of $(C_4H_6O_4)_2 \cdot Zn \cdot 2H_2O$ were added to the mixture and stirred vigorously in a water bath maintained at a constant temperature of 45°C for 3 hours. The stirred solution was transferred to a 200 mL polytetrafluoroethylene (PTFE) high-pressure reactor and reacted in an oven at 150°C for 12 hours. The resulting precipitate was obtained by centrifugation, washed several times with deionized water and anhydrous ethanol, and then dried in a vacuum drying oven at 60°C. The dried precipitate was placed into a crucible and heated in a muffle furnace at a rate of 3 °C/min until it reached a constant temperature of 350 °C, where it was kept for 6 hours. This process resulted in the formation of ZNR.

Preparation of ZnO nanosheets (ZNS). The preparation of ZNS was improved using synthesis methods found in the literature of previous researchers(Hezam, Alsubaie et al. 2021). Dissolved 0.15 g of CTAB and 1.2 g of NaOH in 50 mL of deionized water and dispersed the mixture using ultrasound. The 50 mL aqueous solution of $Zn(NO_3)_2 \cdot 6H_2O$, with a concentration of 0.12 g/mL, was slowly added to the rapidly stirring CTAB-NaOH solution at a rate of 3 mL/min. The mixed solution was then transferred into a PTFE high-pressure reactor and subjected to a reaction in an oven at 100°C for 24 hours. After the reaction, the white precipitate was centrifuged, washed three times with deionized water and anhydrous ethanol, and finally dried in a vacuum drying oven at 60°C for several hours to obtain ZNS.

Amino-functionalization of ZnO-NPs. Amino-functionalized ZnO nanoparticles were synthesized following the modification process described in the literature(Chelladurai, Margavelu et al. 2022). The amino-functionalization of ZnO nanoparticles was achieved using the silane coupling agent 3-APTES. 0.5 g of ZnO-NPs were sonicated and dispersed in 50 mL of the organic solvent DMSO for 45 minutes. Then, 400 μl of 3-APTES was added to the solution and condensed and refluxed at 120°C for 3 hours. The resulting colloidal solution was centrifuged at 12,000 rpm for 20 minutes and then washed with anhydrous ethanol to remove any unreacted material. Finally, the precipitate was dried at 60°C to obtain two distinct morphologies of amino-functionalized ZnO nanoparticles.

Synthesis of antibacterial materials -- ZnO-NPs functionalized by citral. The process of functionalizing ZnO nanoparticles with essential oil was based on methods described in the literature, which was modified briefly(Bravo Cadena, Preston et al. 2018). Firstly, 1 g of amino-functionalized ZnO-NPs and 2 g of excess citral (CIT) were dispersed ultrasonically into 50 mL of anhydrous ethanol. The pH of the solution was adjusted to 8.5 with 1% NaOH and stirred at room temperature for 24 hours. The mixture was then separated from the supernatant by centrifugation, and the precipitate was washed three times with deionized water. Finally, it was dried by ventilation at room temperature to obtain ZnO nanorods (ZNR@C) and ZnO nanosheets (ZNS@C) loaded with citral. At the same time, the commercially available amorphous ZnO-NPs were modified with citral to synthesize SAZ@C as the control group.

2.3 Characterization of antibacterial materials and the comparison and screening of antibacterial properties

The prepared samples were analyzed using standard techniques, including scanning electron microscopy (SEM), zeta potential analysis, thermogravimetric analysis (TGA), instrumental Fourier infrared spectroscopy (FTIR), and N_2 adsorption/desorption thermocline. Some modifications were made based on previous studies.

The dried sample powder was evenly spread on a double-sided copper conductive tape and gold particles were then sprayed onto the sample surface. Finally, the scanning electron microscopy images of the samples were obtained by the hot-field scanning electron microscope (Hitachi Regulus 8100, Japan) at an accelerating voltage of 5 kV(Hou, Weng et al. 2021).

The samples were diluted to a concentration of 1 mg/ml in neutral water (pH-6.5~8.0) and sonicated at 25 °C for 20 minutes to create a high dilution dispersion The particle size distribution characteristics of the samples in the sample jars were determined using particle size meter, and the zeta potential was determined using the zeta potential analyzer (Malvern ZS90, UK) (Sun, Lu et al. 2022).

The samples underwent thermal stability analysis using a thermogravimetric analyzer (NETZSCH STA449C, Germany) under air-filled conditions (60 mL/min) at an elevated heating rate of 10 K/min from 30 to 800°C. The degree of functionalization of the antimicrobial carriers was ultimately evaluated based on the ratio of thermogravimetric loss in the samples(Liu, Li et al. 2022).

A small number of solid samples was separately covered on the surface of ATR diamonds and pressed using a constant pressure jig. The infrared spectra of the samples were measured in transmission mode at a resolution of 4 cm^{-1} by scanning 128 times in the wave number range of 500-4000 cm-1 using a Fourier infrared spectrometer(Nicolet Instrument, Thermo Company, USA)(Hou, Weng et al. 2021).

The samples were pre-treated by degassing in a vacuum at 100°C for 3 hours under the experimental pressure to initial pressure ratio (P/P_0) of 0.01-0.99, and then the N_2 adsorption-desorption isotherms were obtained by conducting nitrogen adsorption-desorption experiments by an automatic adsorption analyzer at 77K (Bayer BELSORP-mini, Japan) (Hou, Weng et al. 2021).

After conducting the thermogravimetric analysis (TGA) assay, ZNR@C (60.35%) and ZNS@C (54.13%), which had higher citral loading, were selected to determine their antimicrobial activity. The two antibacterial materials were dispersed into TSB using ultrasonication. Five concentrations (0.05, 0.1, 0.2, 0.4, and 0.8 mg/mL) of suspensions containing nano-antibacterial substances were prepared and placed in test tubes. The tubes were inoculated with 100 μL of *E. coli* culture solution, resulting in an initial density of 10^6 CFU/mL of *E. coli* liquid. The tubes were placed in a microbial culture shaker and incubated at 37°C for 24 hours at 275 rpm. The optical density (OD) of *E. coli* was determined after incubation using the spectrophotometer(Thermo-Multiskan FC, US) set at 600 nm. The number of *E. coli* colonies was determined using the dilution coating plate method, and the counts were transformed to log10 CFU/mL(Sysel, Dunphy et al. 2021). The control group is a blank control group with no samples added. All of the experimental treatments mentioned above were repeated at least three times. The formula of antibacterial rate(N) is as follows:

$$N = \left(1 - \frac{A}{B}\right) \times 100\%$$

A: Number of sample colonies;

B: Number of colonies in control group.

2.4 Study of antimicrobial activity and slow-release performance applications of antimicrobial materials -- ZNR@C

Determination of in vitro antibacterial activity of ZNR@C. According to the growth curve of *E. coli* OD values, the antibacterial efficacy of antibacterial nanomaterials was determined. A concentration of 0.1 mg/mL of ZNR@C was added to a 10 mL solution of *E. coli* with a density of 10^6 CFU/mL. After repeated mixing with an oscillator, the tubes were placed in a microbiological culture shaker and incubated at 37°C for 24 hours at 275 rpm. Finally, the absorbance of the treated *E. coli* was measured at 600 nm using enzymoleter. Citral and ZNR were used as control samples. All experiments were conducted three times.

Afterward, a more visual method was used to assess and compare the antimicrobial efficacy of the prepared nano-antibacterial materials by observing the number of colonies. Subsequently, the bacterial solution that was treated as described above was diluted by a factor of 100 and then inoculated onto TSA plates. The plates were then incubated at a constant temperature of 37°C for 24 hours. The resulting number of colonies on the plate was recorded.

Determination of the slow-release properties of citral in ZNR@C under varying pH conditions. After determining the antibacterial activity of the three antimicrobial materials, ZNR@C was selected due to its superior antibacterial abilities. Fifty milligrams of ZNR@C were added to 30 mL of phosphate buffer solution at the appropriate pH value and stirred continuously at 200 rpm. Every 2 hours, a 3 mL sample solution was taken. The absorbance was measured using UV-visible spectrophotometer(UV1800PC, China), and the release of citral in the antibacterial material was calculated by substituting it into the standard curve of citral(Kumari, Raza et al. 2021).

To examine the prolonged bacterial inhibition efficacy of citral-functionalized zinc oxide porous nanorods, we stowed ZNR@C and citral at room temperature 25°C protected from light for 5, 10, 20, 30 and 60 days, respectively, and then determined their growth inhibitory effects on *E. coli*. For specific methods, refer to the above antibacterial operation procedure for ZNR@C and ZNS@C.

2.5 Study on bacteriostatic mechanism

In order to investigate the antibacterial mechanism of antibacterial material, scanning electron microscopy was used to observe the morphology of *E. coli* before and after ZNR@C treatment. The procedure was as follows: firstly, ZNR@C was added to the *E. coli* suspension and incubated for 24 hours. The suspension was then incubated at 37°C for 24 hours. After incubation, 1 mL of the suspension was centrifuged at 4000 rpm for 10 minutes, and the supernatant was discarded. Then, the bacterial solution was mixed with a 2.5% glutaraldehyde aqueous solution and left to fix overnight. Next, it was washed more than three times with sterile PSB buffer at pH 7.2-7.4. Finally, the solution was dehydrated using various concentrations of ethanol solution (30%, 50%, 70%, 90%, 100%). Samples were prepared by adding 500 μL of anhydrous ethanol, and 10 μL of the samples were air-dried on sterile slides for observation of cell morphology under SEM.

2.6 Data Analysis

Plots were created using Origin 2021 software, and experimental data were analyzed using SPSS 20.0 software (version 20.0; SPSS Inc., Chicago, IL, USA) with one-way ANOVA. Statistical significance was determined at a test level of $p < 0.05$.

3. Results and Discussion

Figure 1 illustrates the preparation process of ZnO nanorods and provides the specific experimental procedure. The synthesis mechanism of ZnO nanorods can be described by the following equation:

$$C_4H_6O_4{\cdot}Zn{\cdot}2H_2O \rightarrow Zn^{2+} + 2CH_3COO^- \quad (1)$$

$$nNH_3 \cdot H_2\ 0 \rightarrow nNH_4^+ + nOH^- \quad (2)$$

$$Zn^{2+} + 4OH^- \rightarrow Zn(OH)_4^{2-} \rightarrow ZnO + H_2O + 2OH^- \quad (3)$$

Because β-cyclodextrin has the hydrophilic outer surface and hydrophobic inner surface, a large amount of Zn^{2+} and OH^- both gather in the inner cavity of cyclodextrin due to electrostatic interaction force under certain hydrothermal conditions, and then nucleate uniformly, grow slowly. Besides, because of the interaction between $Zn(OH)_4^{2-}$ ions and surfactant CTA^+ ions, the hydrophobic CTA^+ attaches to the negatively charged ionic surface, which hinders the attachment of $Zn(OH)_4^{2-}$ ions in space and charge, thus inhibiting the disordered growth of ZnO(Ouyang, Ren et al. 2021).

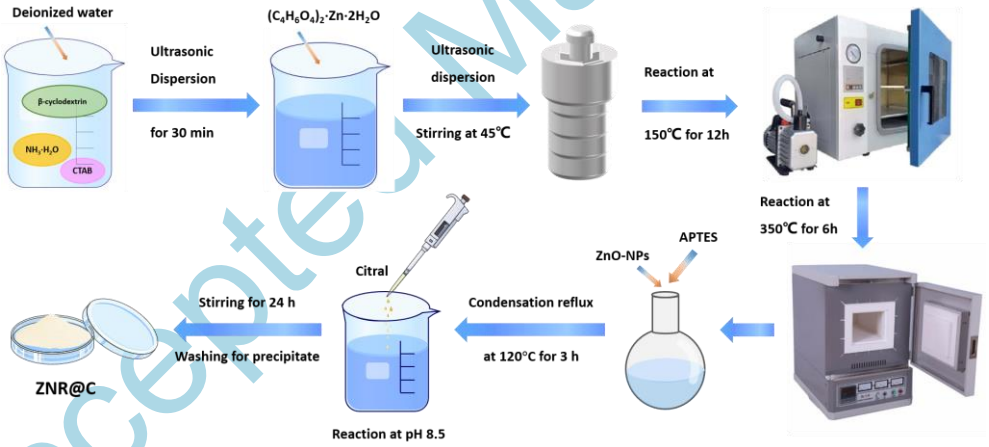

Figure 1. Synthesis of ZNR@C

Figure 2 illustrates the process for preparing oxidative nanosheets and the specific experimental procedure. The synthesis mechanism of ZnO flakes follows the following equation:

$$Zn^{2+} + 2OH^- \rightarrow Zn(OH)_2\downarrow \quad (4)$$

$$Zn(OH)_2 + 2OH^- \rightarrow Zn(OH)_4^{2-} \quad (5)$$

$$Zn(OH)_4^{2-} \rightarrow ZnO + H_2O + 2OH^- \quad (6)$$

The above equation illustrates the importance of OH^- in initiating the reaction and controlling the reaction rate. The above reactions (4) and (5) occur faster when there are more OH^- in the solution and

the reaction rate (6) increases. Firstly, CTAB is ionized into CTA^+, and $Zn(OH)_4^{2-}$ ions bonded with CTA^+. The negatively charged ions in the reaction system were well condensed on the positively charged ion surface through electrostatic interaction. Hydrophobic CTA^+ adheres to the surface of positively charged ions, hindering the adhesion of $Zn(OH)_4^{2-}$ ions in space and charge, thus inhibiting the disordered growth of zinc oxide and forming a sheet form(Guo, Fu et al. 2014).

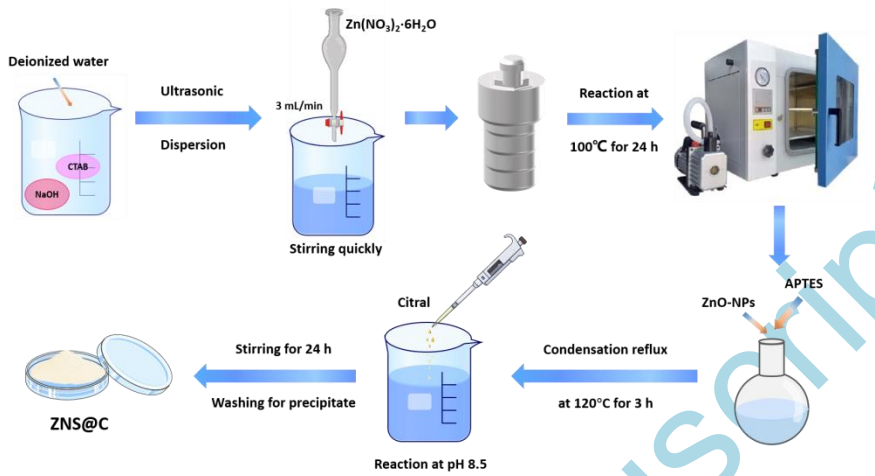

Figure 2. Synthesis of ZNS@C

Figure 3 shows the morphology of ZnO nanorods, nanosheets, and commercial available disordered nanoparticles before and after functionalization as observed via scanning electron microscopy. The ZnO nanorods, before and after functionalization (Figure 3 A, B), exhibit a uniformly shaped rod-like structure with a length ranging from 5-10 μm and a bottom diameter of approximately 500 nm-3 nm. The ZnO nanosheets, both before and after functionalization (Figure 3 C, D), exhibit a uniformly shaped flake morphology, with a length ranging from 3 μm to 8 μm and a width of 500 nm. This size and morphology are consistent with those previously reported(Hezam, Alsubaie et al. 2021). The commercial available disordered ZnO nanoparticles, both before and after functionalization (Figure 3 E, F), exhibited variable morphology with non-uniform particle sizes, with granular, blocky, and needle-like morphologies. Comparison before and after functionalization revealed that amino functionalization did not affect the structure of the materials, which confirms that subsequent modification treatments do not alter the integrity and morphology of the nanomaterial matrix.

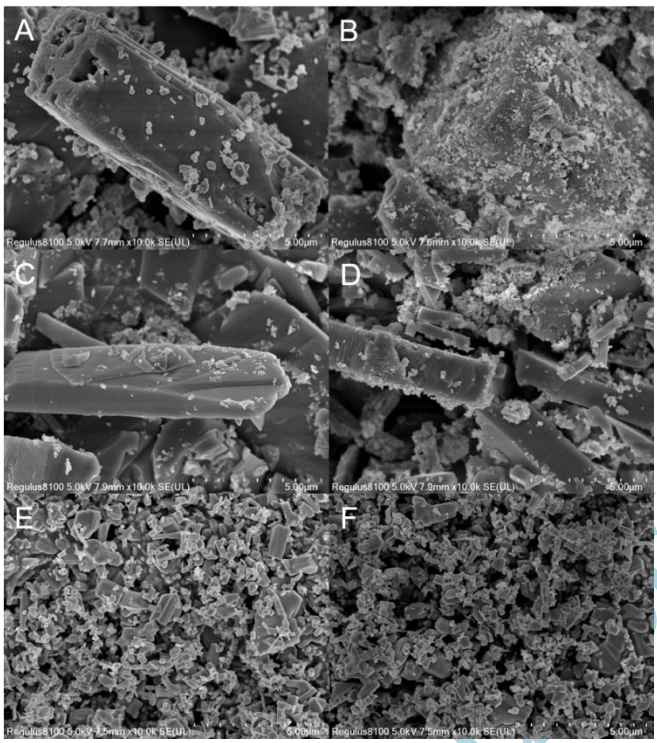

Figure 3. Scanning Electron Microscopic (SEM) images of the ZnO nanorods(A, B), nanosheets(C, D), and commercial nanoparticles(E, F) before and after functionalization

The zeta potentials of ZnO nanomaterials are presented in Figure 4, both before and after functionalization with the amino group and essential oil molecules. The zeta potential is a crucial parameter for predicting the surface charge of nanomaterials. As can be seen from the figure, ZnO nanomaterials functionalized with positively charged 3-APTES aminosignificantly increase from smaller positive charge numbers to large positive charge numbers(Rokicka-Konieczna, Wanag et al. 2020, Mahalanobish, Kundu et al. 2022). After citral was chemically bonded to the ZnO nanomaterials, the surface charge of the material was slightly reduced. The reason for this may be that certain active ingredients, such as essential oils, produce negative charges after modifying the nanocarriers, thereby decreasing the zeta potential of the ZnO nanomaterials.(Chen, Ference et al. 2020).

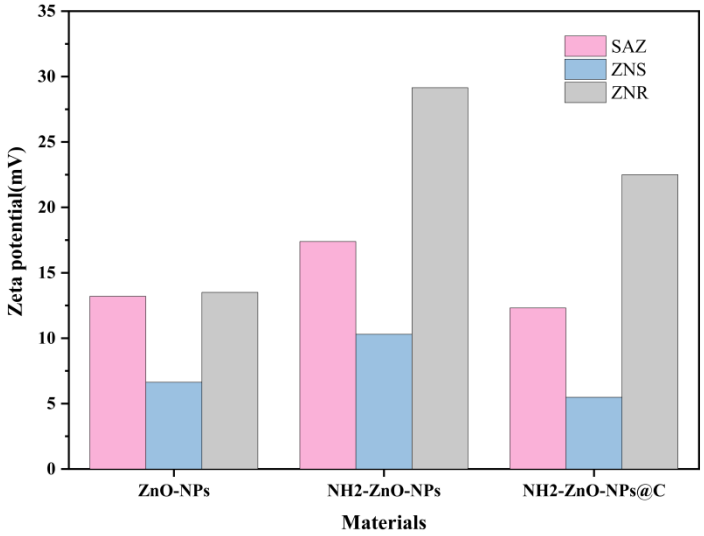

Figure 4. Zeta potential of self-synthesized ZnO nanorods, self-synthesized ZnO nanosheets, and commercial ZnO nanoparticles before and after modification

Figure 5 displays the thermogravimetric analysis curves of ZNR, ZNS, and ZAS, as well as these ZnO-NPs after amino functionalization and citral modification. On account of the greater volatility of

citral under high thermal conditions, thermogravimetric curves can be used to determine the total amount of citral bonded to the nanocarriers. As depicted in the figure, the weight loss curve of unmodified ZnO nanocarriers exhibits only one stage, namely a slight decrease in the weight of ZnO nanocarriers with a minor weight loss within the experimental temperature range. This can be ascribed to the small amount of water molecules absorbed and residual reaction solvent during the synthesis of the nanocarriers.(Rotjanasuworapong, Lerdwijitjarud et al. 2021). Similar to the unmodified material, the antimicrobial carrier functionalized with citral showed a weight reduction in the preliminary stage before reaching 150°C. It is conjectured that the phenomenon is likely due to the thermal evaporation of adsorbed water or solvent on its surface. During the second stage (200 - 450°C), the weight loss of the materials was mainly caused by the decomposition of the citral bonded to the carriers, which simultaneously proved that citral was successfully bonded onto the surface of ZnO-NPs(Sun, Lu et al. 2022). From the thermogravimetric curves, it is evident that ZNR exhibits the highest degree of citral functionalization (60.35%), followed by ZNS (54.13%). SAZ had the lowest degree of essential oil functionalization (15.63%) due to its variable morphology, fewer internal pores, and uneven pore size. Therefore, subsequent characterization and experiments were conducted on ZNR and ZNS.

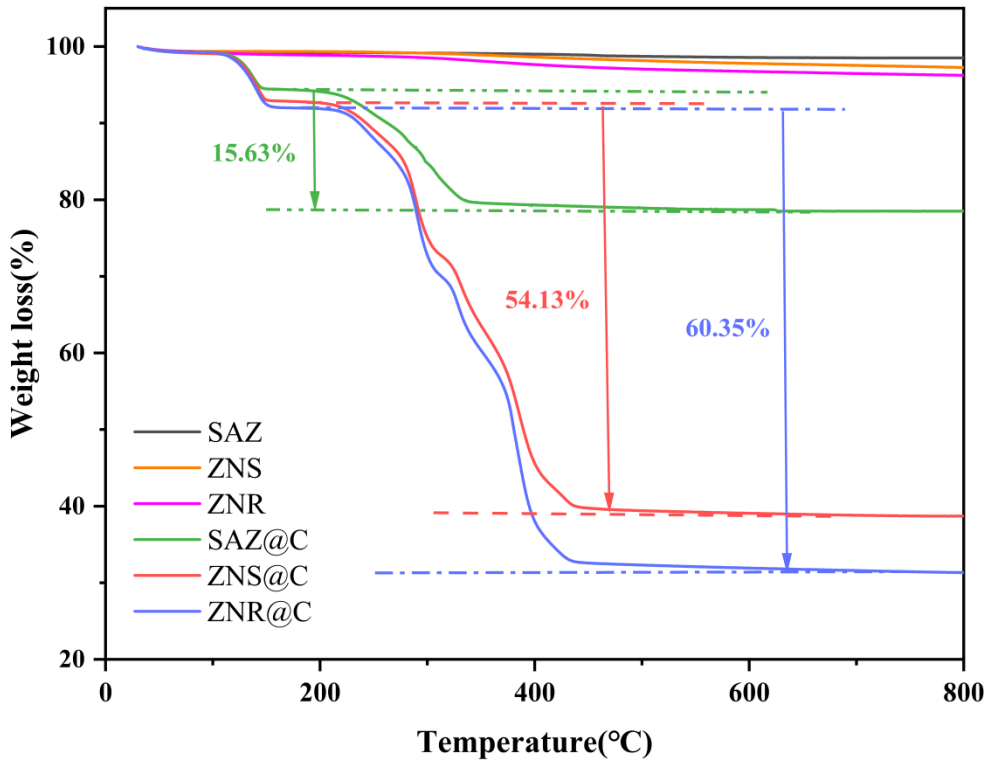

Figure 5. TGA curve of ZNRs， ZNSs, and SAZs before and after functionalization

The infrared spectra of citral, ZNS, and ZNR materials of unmodified and citral-functionalized are illustrated in Fig. 6. FTIR analysis revealed that the peaks at wavelengths 581 and 602 cm^{-1} for unmodified and citral-functionalized ZNS and ZNR corresponded to the stretching of the Zn-O bond. The value of these peaks may vary between 430 and 610 cm^{-1} due to the different synthesis methods of the ZnO-NPs(Sharma and Garg 2022). ZNR and ZNS exhibit a wide absorption peak at 3356 cm^{-1}, which is likely associated with the characteristic absorption of the hydroxyl group in ZnO-NPs(Hong, Li et al. 2009). In the spectra of citral, the FTIR spectral peaks near 2918 cm^{-1} and 2858 cm^{-1} are attributed to the stretching vibrations of CH_3 and CH_2, respectively; the absorption bands at 1671 and 1717 cm^{-1} are attributed to the stretching vibrations of C=C and C=O, respectively; the absorption

bands at 1438 and 1192 cm^{-1} are attributed to the coupling of bending vibrations and C-O stretching vibrations in the OH plane(Tian, Lu et al. 2018). In ZNS@C and ZNR@C, the characteristic bands of ZnO-NPs were observed at 581 cm^{-1} and 602 cm^{-1} , and the relevant characteristic bands of citral were also detected. These observations of these characteristic peaks indicated the successful synthesis of antimicrobial materials ZNS@C and ZNR@C.

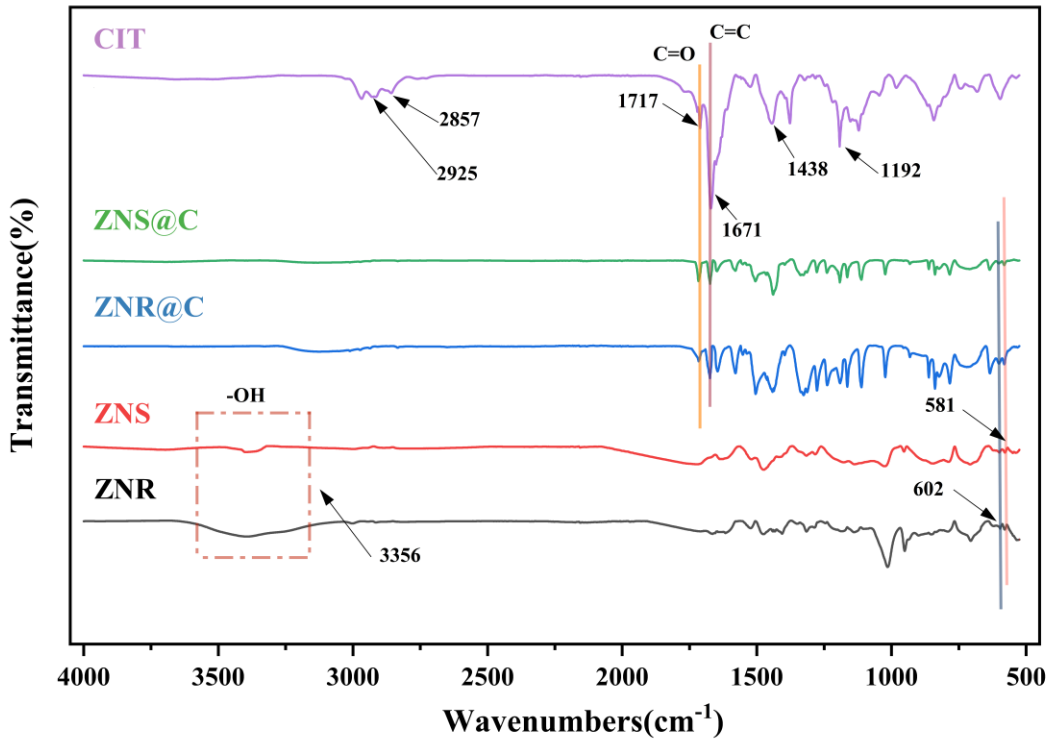

Figure 6. FT-IR of ZNRs, ZNSs before and after functionalization

To gain a deeper understanding of the structure and porosity of ZnO nanoparticles, we analyzed ZNR and ZNS using N_2 adsorption-desorption isotherms (Figure 7). According to the IUPAC classification rules, ZnO-NPs with various morphologies at high relative pressures exhibit V-shaped isotherms and H3-type hysteresis lines (P/P_0 ranging from 0.1 to 1). The reason is that these materials are non-porous or macroporous, while ZnO-NPs are characterized by a homogeneous structure(Liu, Fan et al. 2009, Ouyang, Ren et al. 2021). The synthesized ZNR is a macroporous material, as determined by Fig. 3A and B, while ZNS is a nonporous material, as shown in Fig. 3C and D. Furthermore, the pore size distribution of ZNR is wider than that of ZNS. The pore size distribution of ZNS ranges mainly between 0-10 nm, while that of ZNR is mainly distributed between 0-20 nm and 200-400 nm. The number of pores in ZNR is more, indicating that it has a larger pore volume to accommodate citral. The ZnO-NPs binded with essential oil molecules, as shown in Figure 7C, exhibit a significant reduction in pore volume, which laterally confirms the thermogravimetric curve results, and that ZNR has the highest binding rate of citral.

It can be seen from Table 1 that the specific surface area, average pore size, and pore volume of ZnO nanoparticles with different morphologies exhibited a decreasing trend before and after modification. This phenomenon could be attributed to the binding of citral, which occupies the pores and reduces their parameters, in agreement with the previous trend of pore parameter changes in essential oil molecules functionalized nanomaterials in the literature(Lu, Li et al. 2023).

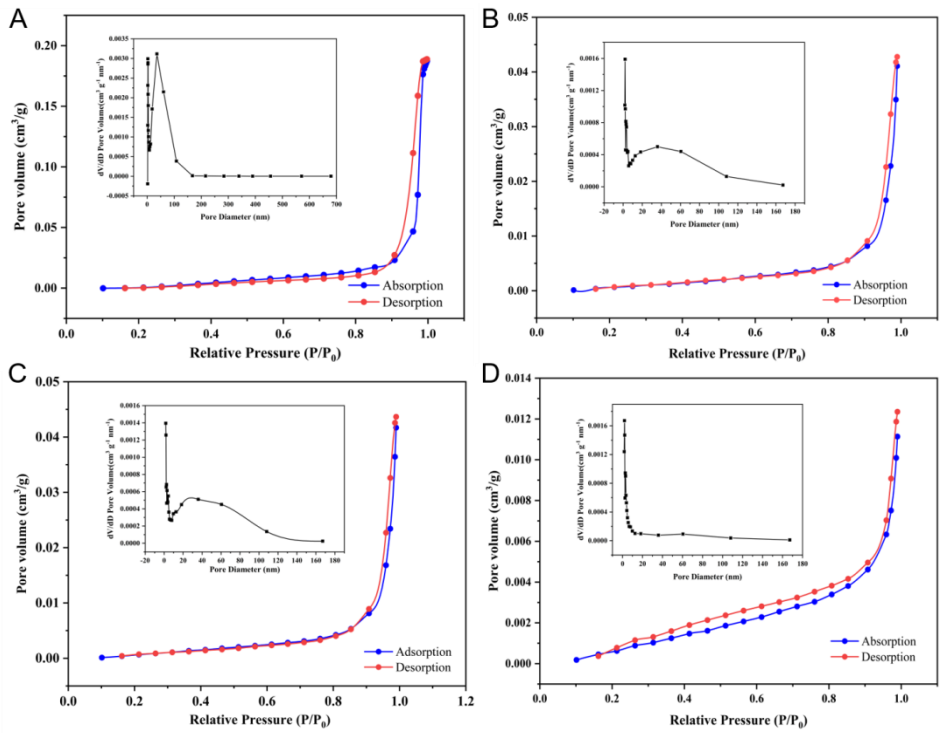

Figure 7. N_2 adsorption-desorption and the pore size comparison of ZNR(A), ZNS(B), ZNR@C(C) and ZNS@C(D)

Materials	Surface Area (m^2/g)	Average pore Diameter(nm)	Pore Volume (cm^3/g)
ZNR	38.79	62.25	0.9364
ZNS	25.14	33.95	0.2134
ZNR@C	17.67	37. 53	0.3075
ZNS@C	11.56	26.17	0.0843

Table 1. The pore structural parameters of ZNSs and ZNRs

The antimicrobial activity of the materials was evaluated by determining the MIC (minimum inhibitory concentration) against representative foodborne microorganisms such as *E. coli*. Figure 8 displays the growth inhibition rates of *E. coli* following 24 hours of treatment with varying concentrations of ZNR, ZNS, ZNR@C, and ZNS@C in comparison to *E. coli*. In Figure 8A, we compared the effects of two unmodified antimicrobial carriers on the growth of *E. coli*. Both carriers showed low inhibition in the range of 0.05 mg/mL to 0.8 mg/mL. The antibacterial property is attributed to the fact that zinc oxide nanomaterial itself is an inorganic metal antimicrobial agent, which can disrupt cell membranes(Gharpure and Ankamwar 2020), bind to protein DNA, generate reactive oxygen species(Saha, Debanath et al. 2020), interfere with the amplification process of bacterial DNA to alter gene expression, and have a direct bactericidal effect on Gram-negative bacteria such as *E. coli*. However, there was no significant difference in the inhibition ability of ZNR and ZNS at the same concentrations, indicating that the two initial morphologies had little effect on the antimicrobial capacity. ZNR@C exhibits stronger antibacterial properties than ZNR in Figure 8B. ZNR@C completely inhibited the growth of *E. coli* in the concentration range of 0.2 mg/mL to 0.8 mg/mL. Whereas ZNR partially inhibited the growth of *E. coli* within the concentration range of 0.05 mg/mL to 0.1 mg/mL, the inhibition decreased from 88% to 3% as the concentration decreased. These findings are consistent with previous studies(Lu, Li et al. 2023). Figure 8D shows that the

antibacterial effect of ZNS@C, which did not achieve 100% inhibition of *E. coli* growth at concentrations of 0.2 mg/mL and below, is slightly inferior to that of ZNR@C. The main reasons for this are as follows: on the one hand, the binding rates of citral to ZNR and ZNS is different, as illustrated in Figure 5.; on the other hand, the surface of the ZnO-NPs carriers after citral functionalization was positive charged, and the positve value was larger than that of ZNS@C, while the surface of *E. coli* cells were negatively charged, so the electrostatic interaction force between ZNR@C and *E. coli* was stronger than that of ZNS@C. The antimicrobial activity of ZnO nanocarriers functionalized with citral is primarily soursed from the interaction between citral with cell membranes(Kachur and Suntres 2020), leading to the leakage of contents and disruption of cell integrity. Ultimately, this results in cell lysis and death.

The antimicrobial activity of carriers is influenced by various factors such as morphology, particle size, pore size, and essential oil loading. These factors predominantly affect the surface potential of the newly synthesized nanomaterials and the loading of antimicrobial compounds so as affect the antibacterial capacity(Velumani, Thiruppathi et al. 2022). Thus, the ZNS@C could more easily attach to the cell surface and exert its bacteriostatic effect and ZNR@C was selected for subsequent in vitro antimicrobial experiments, as well as long-lasting bacterial inhibition and slow-release experiments.

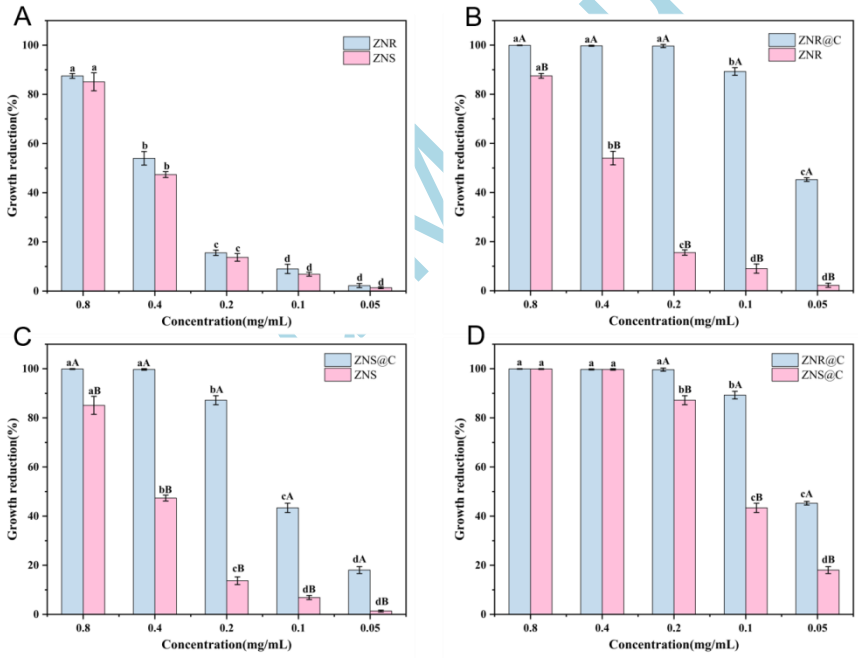

Figure 8. The effects of different concentrations of antibacterial carriers - ZNR, ZNS (A), and citral-functionalized antibacterial materials - ZNR@C and ZNS@C(B, C, D,) on the growth rate of *E. coli* ($p < 0.05$).

The results of the in vitro antimicrobial activity of ZNR@C are presented in Figure 9. The inhibitory effect of the three samples on the growth of *E. coli* was demonstrated in 9A by measuring the OD values of *E. coli* suspensions treated with ZNR, ZNR@C, and CIT. The bacterial inhibition of ZNR@C was not significant during the 0-4 hour interval, probably due to the pH dependence of the controlled release of citral from this material. During the 4-hour duration of action, *E. coli* produced acidic by-products to rapidly decrease the pH, at which the imine bonds in ZNR@C were only marginally broken, releasing a small number of citral. During the 4-24 hour interval, ZNR exhibited some inhibitory ability, but it was weaker than that of the ZNR@C antimicrobial material. The trend and OD values of the bacterial solutions treated with ZNR@C and citral were approximately the

same, indicating that the synthesized antimicrobial material, ZNR@C, owes its inhibitory ability mainly to the presence of citral.

It can also be directly observed from Figure 9B that the antibacterial effect of the sample material on *E. coli* is as follows: within the concentration range of 0.2-0.8 mg/mL, ZNR@C has the strongest antibacterial ability and achieves complete inhibition. Compared to the high volatility and potent antimicrobial properties of pure citral, ZNR@C demonstrated superior stability and antimicrobial properties at different concentrations (0.1 mg/mL and 0.05 mg/mL).

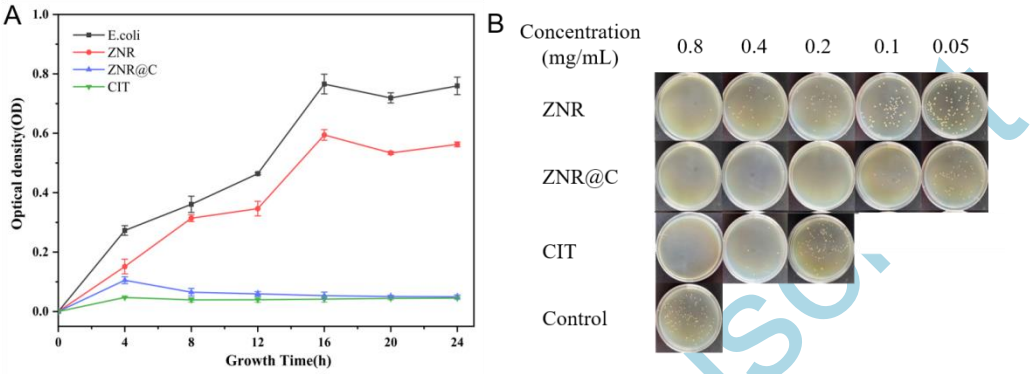

Figure 9. The comparison of antibacterial properties of antibacterial materials at 0.01mg/mL concentration(A) and results of antibacterial coating plates at different concentrations of ZNR@C(B)

Figure 10A represents the pH change of *E. coli* in TSB culture medium over 24 hours. It can be observed that the pH of *E. coli* in TSB initially decreased sharply, then leveled off, and finally showed a slow increase as the incubation time increased. In Fig. 9, the antimicrobial effect of ZNR@C was not evident within the first 0-4 hours. The reason for this may be the rapid proliferation of *E. coli* cells due to nutrient enrichment, resulting in the production of metabolites, which in turn caused a rapid drop in system pH. Based on the fit, the standard curve of citral was calculated in figure 10B as $y = 0.1070 + 1.8905\ x$, $R^2 = 0.9991$. Figure 10C shows the release rate of citral from ZNR@C at different pH levels (7.4, 6.5, 5.0). As the system becomes more acidic, the material releases a greater amount of essential oil molecules and the release rate is faster. At pH 5.0, the release of essential oil molecules from the material increased rapidly to 80% within 12 hours, and the maximum release exceeded 90%. In contrast, at a pH of 7.4, the release of essential oil molecules from the material remained at no more than 10% after 24 hours. As the pH decreases and acidification increases, the imine bond connecting the amino group to the citral is broken, releasing a significant amount of essential oil molecules to produce an antimicrobial effect(Zeng, Liu et al. 2017, Ren, Li et al. 2021). Starting from the 5th hour, the pH of the bacteria's growth environment reached between 5-6, when combined with Fig. 10C, this pH condition is favorable for the release of citral. The growth rate of the *E. coli* colony slowed down between the 15th-24th hour due to the depletion of nutrients in the medium and the accumulation of harmful metabolites, *E. coli* continued to a later stage, which may result in apoptosis due to the discharge of contents, and the pH value gradually increased to 5.86.

Revised 2: It has been experimentally confirmed that ZNR@C, an antimicrobial material, functions as a pH-responsive essential oil controlled-release system. In this system, a small number of metabolites is produced when there is a low concentration of *E. coli* in the system, which lowers the pH slightly, opens a small number of imine bonds to release essential oil molecules for inhibiting the bacteria; while a large number of metabolites produced by *E. coli* can significantly lower the pH of

the system, and the imine bonds are sufficiently destroyed to release a large number of essential oil molecules for inhibiting the bacteria(LI Xiang-Zi 2018, Lu, Li et al. 2023).

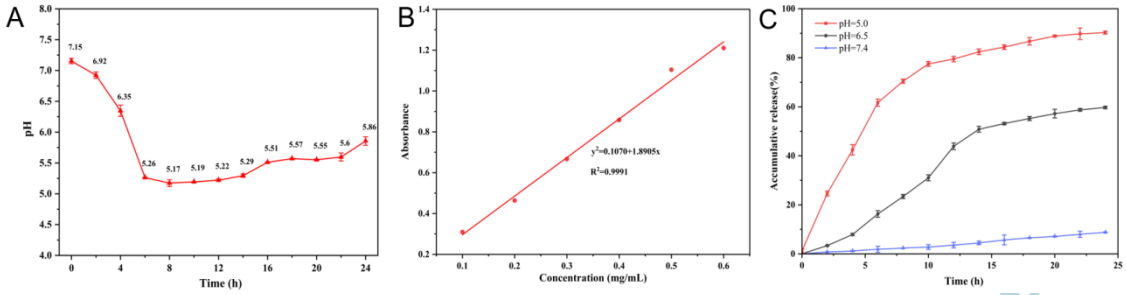

Figure 10. The slow-release properties of ZNR@C antimicrobial materials

(Notes: A represents the pH change of *E. coli* grown in TSB. B represents the standard curve of citral. C represents the release curve of citral from ZNR@C material.)

Figure 11 displays the growth inhibition rates of ZNR@C and citral against *E. coli* on different days of placement (5, 10, 20, 30, and 60 days). The results indicate that ZNR@C exhibits excellent long-lasting bacterial inhibition ability. It inhibited 100% of *E. coli* growth on day 10 and maintained 58.17% inhibition even on day 60. This performance surpasses that of synthetic antimicrobial materials previously reported in the literature(Si, Gao et al. 2021). This suggests that citral is not simply diffusing freely onto the ZNR, but rather forming strong covalent bonds with the nanomaterials(Peña-Gómez, Ruiz-Rico et al. 2019). The decrease in bacterial inhibitory ability observed between day 20 and day 60 can be attributed to the collapse of the microstructure of the ZnO-NPs nanocarriers and the dilution of the essential oil concentration due to its hygroscopicity. In contrast, pure citral completely evaporated on day 20 and therefore could not exert its excellent bacteriostatic effect against *E. coli*.

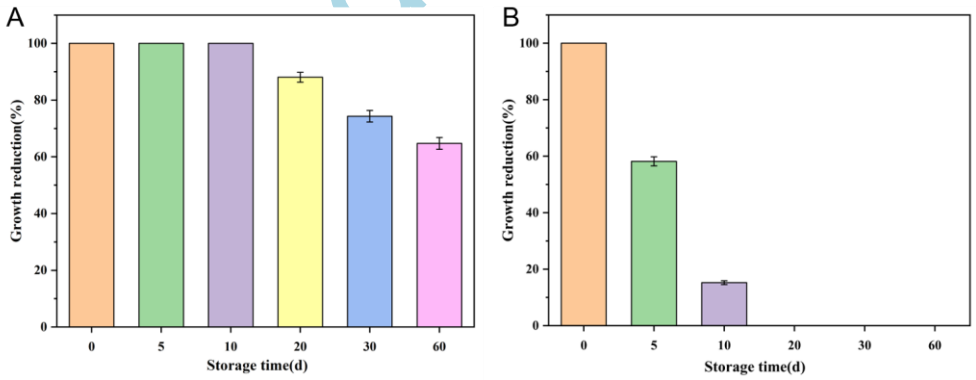

Figure 11. The growth reduction of antibacterial materials with different storage days on *E.coli*: ZNR@C(A) and CIT(B)

SEM analysis of *E. coli* before and after ZNR@C treatment was performed to further investigate the antimicrobial mechanism of the antimicrobial material. As shown in Figure 12, the surface of *E. coli* before antimicrobial treatment appeared relatively smooth, and the cell membrane and cell wall were intact, with the complete cell morphology of *E. coli*. This is consistent with the pictures shown in the referenced literature. After the antimicrobial treatment, the cell surface appeared concave and exhibited partial contraction, which may be due to the interaction between citral with the lipids present on the bacterial cell membrane, increasing the permeability of the cell membrane, leading to the leakage of the cell and subsequently affecting bacterial activity(Firmanda, Fahma et al. 2023).

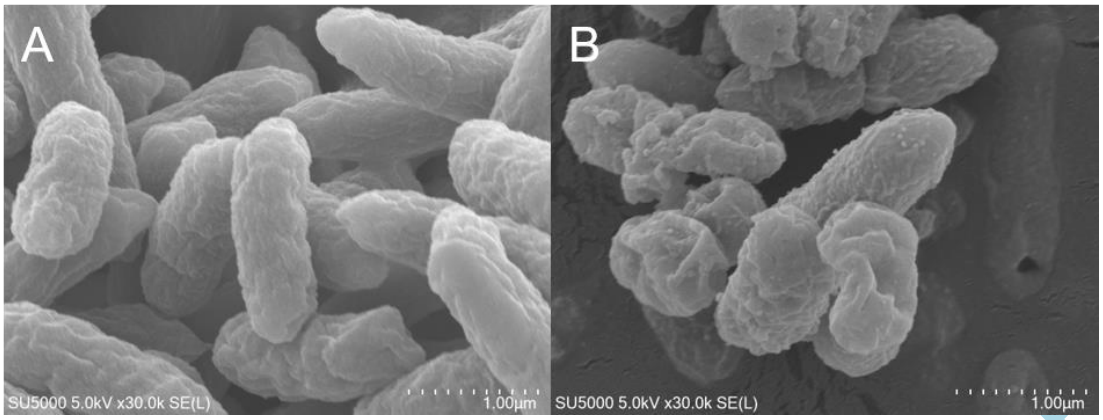

Figure 12. Scanning electron microscopy (SEM) of *E. coli* before and after being treated with ZNR@C

4. Conclusion

After screening by experiments, this study synthesized a novel zinc oxide porous nanorod (ZNR) using the synthetic template (β-cyclodextrin) to allow aggregation of zinc oxide nanorods to grow and the surfactant (CTAB) to restrict its growth direction. And then ZNR was modified with 3-APTES amino functionalization and covalently bound to citral via pH-sensitive imine bonds to obtain a high-quality, pH-responsive antimicrobial material (ZNR@C). The results revealed that this loading mode of chemical bonding could effectually decrease the volatilization of citral and enhance the utilization of its antimicrobial activity. The positive charge on the surface of the synthesized ZNR@C can attract the negatively charged Escherichia coli, so as to achieve a better antibacterial effect. The weakly acidic metabolites produced during the growth of *E. coli* in the system of the novel antimicrobial material ZNR@C can lower the pH of the system, break down the imine bond, and release the essential oil to inhibit bacteria. The more *E. coli* there are, comparatively the pH of the system becomes more acidic, the higher the rate of imine bond disruption of ZNR@C is, the more essential oil molecules are released, and the better the antibacterial effect is, thus confirming that this novel antimicrobial material, ZNR@C, is a pH-responsive essential oil-controlled-release system that effectively inhibis *E. coli*.

In conclusion, this study presents a feasible method for immobilizing beneficial natural antimicrobial compounds onto nanocarriers through covalent bonding, provides new insights for the research and development of food packaging materials utilizing natural essential oils, increases the application prospects of natural antimicrobial essential oils in the food antibacterial field (e.g., bacterial filtration of liquid foods), and provides a theoretical foundation for the application of this innovative antimicrobial material in reducing the risk of foodborne illness.

AuthorContributions

Ya-nan Fan: Conceptualization, Data curation, Formal analysis, Writing – original draft, Writing – review & editing, Visualization, Software. **Qixiang Xu**: Conceptualization, Data curation, Formal analysis, Writing – original draft, Visualization**. Ke-yu Ren**: Software, Writing – review & editing, Visualization. **Meng-ge Zhai**: Conceptualization, Methodology, Resources. **Guo-zheng Xing**: Conceptualization, Methodology, Data curation. **Yi-shan Song**: Supervision, Writing – review & editing, Project administration, Funding acquisition. **Yongheng Zhu**: Visualization, Supervision, Writing – review & editing, Project administration, Funding acquisition.

Acknowledgments

We greatly appreciate the financial support from the National Natural Science Foundation of China (32272399).

Funding

This research was funded by National Natural Science Foundation of China (32272399).

Declaration of competing interest

The authors declare that they have no known competing financial interests or persona relationships that could have appeared to influence the work reported in this paper.

Reference

Al-Maqtari, Q. A., A. Rehman, A. A. Mahdi, W. Al-Ansi, M. Wei, Z. Yanyu, H. M. Phyo, O. Galeboe and W. Yao (2021). "Application of essential oils as preservatives in food systems: challenges and future prospectives - a review." Phytochemistry Reviews 21(4): 1209-1246.

Aladhadh, M. (2023). "A Review of Modern Methods for the Detection of Foodborne Pathogens." Microorganisms 11(5).

Bravo Cadena, M., G. M. Preston, R. A. L. Van der Hoorn, H. E. Townley and I. P. Thompson (2018). "Species-specific antimicrobial activity of essential oils and enhancement by encapsulation in mesoporous silica nanoparticles." Industrial Crops and Products 122: 582-590.

Chelladurai, M., G. Margavelu, S. Vijayakumar, Z. I. González-Sánchez, K. Vijayan and R. Sahadevan (2022). "Preparation and characterization of amine-functionalized mupirocin-loaded zinc oxide nanoparticles: A potent drug delivery agent in targeting human epidermoid carcinoma (A431) cells." Journal of Drug Delivery Science and Technology 70.

Chen, P., C. Ference, X. Sun, Y. Lin, L. Tan and T. Zhong (2020). "Antimicrobial Efficacy of Liposome-Encapsulated Citral and Its Effect on the Shelf Life of Shatangju Mandarin." J Food Prot 83(8): 1315-1322.

Chen, X., S. Shang, F. Yan, H. Jiang, G. Zhao, S. Tian, R. Chen, D. Chen and Y. Dang (2023). "Antioxidant Activities of Essential Oils and Their Major Components in Scavenging Free Radicals, Inhibiting Lipid Oxidation and Reducing Cellular Oxidative Stress." Molecules 28(11).

Costa, B. A., M. P. Abucafy, T. W. L. Barbosa, B. L. da Silva, R. B. Fulindi, G. Isquibola, P. I. da Costa and L. A. Chiavacci (2023). "ZnO@ZIF-8 Nanoparticles as Nanocarrier of Ciprofloxacin for Antimicrobial Activity." Pharmaceutics 15(1).

Czyzowska, A. and A. Barbasz (2022). "A review: zinc oxide nanoparticles - friends or enemies?" Int J Environ Health Res 32(4): 885-901.

Du, J., Y. Zhang, M. Qv, K. Li, X. Yin, B. K. Sorrell, M. Wei and C. Ma (2019). "The effects of ZnO nanoparticles on leaf litter decomposition under natural sunlight." Environmental Science: Nano 6(4): 1180-1188.

Firmanda, A., F. Fahma, E. Warsiki, K. Syamsu, I. W. Arnata, D. Sartika, L. Suryanegara, Qanytah and A. Suyanto (2023). "Antimicrobial mechanism of nanocellulose composite packaging incorporated with essential oils." Food Control 147.

Gharpure, S. and B. Ankamwar (2020). "Synthesis and Antimicrobial Properties of Zinc Oxide Nanoparticles." J Nanosci Nanotechnol 20(10): 5977-5996.

Ghasemy-piranloo, F., F. Kavousi and S. Dadashian (2020). "Comparison for the Production of Essential Oil by Conventional, Novel and Biotechnology Methods." Journal of Essential Oil Research 34(5): 455-478.

Guo, L., S. M. R. Azam, Y. Guo, D. Liu and H. Ma (2022). "Germicidal efficacy of the pulsed magnetic field against pathogens and spoilage microorganisms in food processing: An overview." Food Control 136.

Guo, W., M. Fu, C. Zhai and Z. Wang (2014). "Hydrothermal synthesis and gas-sensing properties of ultrathin hexagonal ZnO nanosheets." Ceramics International 40(1): 2295-2298.

Hailu, W., Y. A. Helmy, G. Carney-Knisely, M. Kauffman, D. Fraga and G. Rajashekara (2021). "Prevalence and Antimicrobial Resistance Profiles of Foodborne Pathogens Isolated from Dairy Cattle and Poultry Manure Amended Farms in Northeastern Ohio, the United States." Antibiotics (Basel) 10(12).

Heras-Mozos, R., R. Hernández, R. Gavara and P. Hernández-Muñoz (2022). "Dynamic covalent chemistry of imines for the development of stimuli-responsive chitosan films as carriers of sustainable antifungal volatiles." Food Hydrocolloids 125.

Hezam, M., M. Q. Alsubaie, A. Algarni, H. Ghaithan, J. Labis and M. Alduraibi (2021). "ZnO

Nanosheet-Nanowire morphology tuning for Dye-sensitized solar cell applications." Chemical Physics Letters **780**.
Hong, R. Y., J. H. Li, L. L. Chen, D. Q. Liu, H. Z. Li, Y. Zheng and J. Ding (2009). "Synthesis, surface modification and photocatalytic property of ZnO nanoparticles." Powder Technology **189**(3): 426-432.
Hou, J., R. Weng, W. Jiang, H. Sun, J. Xia, Y. Liu, J. Sheng and Y. Song (2021). "In-situ preparation of novel sedimentary rock-like Fe3O4 by rice-husk mesoporous silica as templates for effective remove As(III) from aqueous solutions." Journal of Environmental Chemical Engineering **9**(5).
Kachur, K. and Z. Suntres (2020). "The antibacterial properties of phenolic isomers, carvacrol and thymol." Critical Reviews in Food Science and Nutrition **60**(18): 3042-3053.
Kavitha, A., A. Doss, R. P. Praveen Pole, T. P. K. Pushpa Rani, R. Prasad and S. Satheesh (2023). "A mini review on plant-mediated zinc oxide nanoparticles and their antibacterial potency." Biocatalysis and Agricultural Biotechnology **48**.
Khan, Y., H. Sadia, S. Z. Ali Shah, M. N. Khan, A. A. Shah, N. Ullah, M. F. Ullah, H. Bibi, O. T. Bafakeeh, N. B. Khedher, S. M. Eldin, B. M. Fadhl and M. I. Khan (2022). "Classification, Synthetic, and Characterization Approaches to Nanoparticles, and Their Applications in Various Fields of Nanotechnology: A Review." Catalysts **12**(11).
Kumari, P., W. Raza and A. Meena (2021). "Lemongrass derived cellulose nanofibers for controlled release of curcumin and its mechanism of action." Industrial Crops and Products **173**.
Kuttithodi, A. M., A. Narayanankutty, N. U. Visakh, J. T. Job, B. Pathrose, O. J. Olatunji, A. Alfarhan and V. Ramesh (2023). "Chemical Composition of the Cinnamomum malabatrum Leaf Essential Oil and Analysis of Its Antioxidant, Enzyme Inhibitory and Antibacterial Activities." Antibiotics **12**(5).
LI Xiang-Zi, H. P.-J., ZHU Zhen-Duo, ZHU Guo-Xing, SHEN Xiao-Ping, WANG Min, SUN Yu, FENG De-Xiang (2018). "Release Mechanisms and Properties of pH-responsive Drug Nanocarriers." Chinese Journal of Inorganic Chemistry **34**(08): 1399-1412.
Lin, J., H. Meng, X. Guo, Z. Tang and S. Yu (2023). "Natural Aldehyde-Chitosan Schiff Base: Fabrication, pH-Responsive Properties, and Vegetable Preservation." Foods **12**(15).
Liu, Y., W. Li, K. Li, P. K. Annamalai, S. Pratt, M. Hassanpour, H. Lu and Z. Zhang (2022). "Tailored production of lignin-containing cellulose nanofibrils from sugarcane bagasse pretreated by acid-catalyzed alcohol solutions." Carbohydr Polym **291**: 119602.
Liu, Z., T. Fan, D. Zhang, X. Gong and J. Xu (2009). "Hierarchically porous ZnO with high sensitivity and selectivity to H2S derived from biotemplates." Sensors and Actuators B: Chemical **136**(2): 499-509.
Lu, Y., X. Li, J. Xu, H. Sun, J. Sheng, Y. Song and Y. Chen (2023). "Utilizing Imine Bonds to Create a Self-Gated Mesoporous Silica Material with Controlled Release and Antimicrobial Properties." Nanomaterials (Basel) **13**(8).
Mahalanobish, S., M. Kundu, S. Ghosh, J. Das and P. C. Sil (2022). "Fabrication of phenyl boronic acid modified pH-responsive zinc oxide nanoparticles as targeted delivery of chrysin on human A549 cells." Toxicol Rep **9**: 961-969.
Meenu, M., B. Padhan, M. Patel, R. Patel and B. Xu (2023). "Antibacterial activity of essential oils from different parts of plants against Salmonella and Listeria spp." Food Chem **404**(Pt B): 134723.
Mengistu, D. A. and S. T. Tolera (2020). "Prevalence of Microorganisms of Public Health Significance in Ready-to-Eat Foods Sold in Developing Countries: Systematic Review and Meta-Analysis." Int J Food Sci **2020**: 8867250.
Mishra, P. K., H. Mishra, A. Ekielski, S. Talegaonkar and B. Vaidya (2017). "Zinc oxide nanoparticles: a promising nanomaterial for biomedical applications." Drug Discov Today **22**(12): 1825-1834.
Mohamed Abdoul-Latif, F., A. Ainane, I. Houmed Aboubaker, J. Mohamed and T. Ainane (2023). "Exploring the Potent Anticancer Activity of Essential Oils and Their Bioactive Compounds:

Mechanisms and Prospects for Future Cancer Therapy." Pharmaceuticals 16(8).
Nie, Y., Y. Pan, Y. Jiang, D. Xu, R. Yuan, Y. Zhu and Z. Zhang (2023). "Stability and bioactivity evaluation of black pepper essential oil nanoemulsion." Heliyon 9(4): e14730.
Ouyang, Z., P. Ren, D. e. Zheng, L. Huang, T. Wei, C. Yang, X. Kong, Y. Yin, S. He and Q. He (2021). "Hydrothermal synthesis of a new porous zinc oxide and its antimicrobial evaluation in weanling piglets." Livestock Science 248.
Peighambardoust, S., M. Yaghoubi, A. Hosseinpour, K. Alirezalu, M. Soltanzadeh and M. Dadpour (2022). "Development and Application of Dual-Sensors Label in Combination with Active Chitosan-Based Coating Incorporating Yarrow Essential Oil for Freshness Monitoring and Shelf-Life Extension of Chicken Fillet." Foods 11(21).
Peña-Gómez, N., M. Ruiz-Rico, I. Fernández-Segovia and J. M. Barat (2019). "Study of apple juice preservation by filtration through silica microparticles functionalised with essential oil components." Food Control 106.
Ren, G., B. Li, L. Ren, D. Lu, P. Zhang, L. Tian, W. Di, W. Shao, J. He and D. Sun (2021). "pH-Responsive Nanoemulsions Based on a Dynamic Covalent Surfactant." Nanomaterials (Basel) 11(6).
Ren, R., C. Lim, S. Li, Y. Wang, J. Song, T. W. Lin, B. W. Muir, H. Y. Hsu and H. H. Shen (2022). "Recent Advances in the Development of Lipid-, Metal-, Carbon-, and Polymer-Based Nanomaterials for Antibacterial Applications." Nanomaterials (Basel) 12(21).
Rokicka-Konieczna, P., A. Wanag, A. Sienkiewicz, E. Kusiak-Nejman and A. W. Morawski (2020). "Antibacterial effect of TiO2 nanoparticles modified with APTES." Catalysis Communications 134.
Rotjanasuworapong, K., W. Lerdwijitjarud and A. Sirivat (2021). "Synthesis and Characterization of Fe0.8Mn0.2Fe2O4 Ferrite Nanoparticle with High Saturation Magnetization via the Surfactant Assisted Co-Precipitation." Nanomaterials 11(4).
Saha, R. K., M. K. Debanath, B. Paul, S. Medhi and E. Saikia (2020). "Antibacterial and nonlinear dynamical analysis of flower and hexagon-shaped ZnO microstructures." Sci Rep 10(1): 2598.
Samart, S. and S. Chutipaijit (2019). "Growth of pigmented rice (Oryza sativa L. cv. Riceberry) exposed to ZnO nanoparticles." Materials Today: Proceedings 17: 1987-1994.
Sharma, S., K. Kumar, N. Thakur, S. Chauhan and M. S. Chauhan (2019). "The effect of shape and size of ZnO nanoparticles on their antimicrobial and photocatalytic activities: a green approach." Bulletin of Materials Science 43(1).
Sharma, T. and M. Garg (2022). "Optical and morphological characterization of ZnO nano-sized powder synthesized using single step sol-gel technique." Optical Materials 132.
Si, W., Y. Gao, X. Mei, C. Wu, J. Li and J. Zhang (2021). "Mesoporous silica nanoparticles loaded with capsaicin and their oxidation resistance in meat preservation." Food Chem 344: 128737.
Siyadatpanah, A., R. Norouzi, F. Mirzaei, B. F. Haghirosadat, V. Nissapatorn, W. Mitsuwan, M. Nawaz, M. L. Pereira, S. A. Hosseini, M. Montazeri, M. Majdizadeh, R. S. Almeida, M. Hemati, P. Wilairatana and H. D. M. Coutinho (2023). "Green synthesis of nano-liposomes containing Bunium persicum and Trachyspermum ammi essential oils against Trichomonasvaginalis." J Microbiol Immunol Infect 56(1): 150-162.
Soni, A. and G. Brightwell (2022). "Effect of Hurdle Approaches Using Conventional and Moderate Thermal Processing Technologies for Microbial Inactivation in Fruit and Vegetable Products." Foods 11(12).
Sun, H., Y. Lu, J. Sheng and Y. Song (2022). "Zein-Functionalized MCM-41 Silica Nanoparticles with Enzyme-Responsive for Controlled Release in Antibacterial Activity." Coatings 13(1).
Sysel, A. M., M. J. Dunphy and J. A. Bauer (2021). "Antimicrobial properties of diethylamine NONOate, a nitric oxide donor, against Escherichia coli: a pilot study." J Antibiot (Tokyo) 74(4): 260-265.
Tajkarimi, M. M., S. A. Ibrahim and D. O. Cliver (2010). "Antimicrobial herb and spice

compounds in food." Food Control 21(9): 1199-1218.
Tian, H., Z. Lu, D. Li and J. Hu (2018). "Preparation and characterization of citral-loaded solid lipid nanoparticles." Food Chem 248: 78-85.
Velumani, M., G. Thiruppathi, A. Mohankumar, D. Kalaiselvi, P. Sundararaj and P. Premasudha (2022). "Green synthesis of zinc oxide nanoparticles using Cananga odorata essential oil and its antibacterial efficacy in vitro and in vivo." Comp Biochem Physiol C Toxicol Pharmacol 262: 109448.
Vodyashkin, A. A., P. Kezimana, A. A. Vetcher and Y. M. Stanishevskiy (2022). "Biopolymeric Nanoparticles－Multifunctional Materials of the Future." Polymers 14(11).
WANG Xiaodong, K. Y., ZHANG Yanling, Ariunjargal TSOGTBAYAR (2022). "Mechanism of sterilization technology and its application in food field." China Brewing 41(2): 1-8.
Wang Xuewen, Xu Zhengyan, Wang Kaige, Zhang Zhiyong and Z. Wu (2022). "Research Progress of Biosensors Based on Nano-zinc Oxide (Invited)." Acta Photonica Sinica 51(10).
Yin, L., C. Liang, W. Wei, S. Huang, Y. Ren, Y. Geng, X. Huang, D. Chen, H. Guo, J. Fang, H. Deng, W. Lai, S. Yu and P. Ouyang (2022). "The Antibacterial Activity of Thymol Against Drug-Resistant Streptococcus iniae and Its Protective Effect on Channel Catfish (Ictalurus punctatus)." Front Microbiol 13: 914868.
YIN Wanting, L. K., MA Lingjun, CHEN Fang, LIAO Xiaojun, HU Xiaosong, JI Junfu (2023). "Preparation and Stability Analysis of Capsaicin-Loaded Thiolated Chitosan-Zein Nanoparticles." Food Science 44(10): 8-14.
Yoon, J. and S.-G. Oh (2021). "Synthesis of amine modified ZnO nanoparticles and their photocatalytic activities in micellar solutions under UV irradiation." Journal of Industrial and Engineering Chemistry 96: 390-396.
Yu, Z., Q. Li, J. Wang, Y. Yu, Y. Wang, Q. Zhou and P. Li (2020). "Reactive Oxygen Species-Related Nanoparticle Toxicity in the Biomedical Field." Nanoscale Res Lett 15(1): 115.
Zeng, X., G. Liu, W. Tao, Y. Ma, X. Zhang, F. He, J. Pan, L. Mei and G. Pan (2017). "A Drug-Self-Gated Mesoporous Antitumor Nanoplatform Based on pH-Sensitive Dynamic Covalent Bond." Advanced Functional Materials 27(11).
Zhang, X., J. Niu, Z. Zhou, G. Tang, G. Yan, Y. Liu, J. Wang, G. Hu, J. Xiao, W. Yan and Y. Cao (2023). "Stimuli-responsive polymeric micelles based on cellulose derivative containing imine groups with improved bioavailability and reduced aquatic toxicity of pyraclostrobin." Chemical Engineering Journal 474.
Zhang, Z., C. He and X. Chen (2018). "Hydrogels based on pH-responsive reversible carbon-nitrogen double-bond linkages for biomedical applications." Materials Chemistry Frontiers 2(10): 1765-1778.
ZHAO Dongxue, Y. X., LANG Yumiao (2021). "Research Progress of Natural Antibacterial Agents in Food Preservation." The Food Industry 42(07): 204-207.
Zhou, Y., Z. Zhai, Y. Yao, J. C. Stant, S. L. Landrum, M. J. Bortner, C. E. Frazier and K. J. Edgar (2023). "Oxidized hydroxypropyl cellulose/carboxymethyl chitosan hydrogels permit pH-responsive, targeted drug release." Carbohydr Polym 300: 120213.